Lerski et al. EPJ Nonlinear Biomedical Physics (2015) 3:2
DOI 10.1140/epjnbp/s40366-015-0018-0

EPJ Nonlinear Biomedical Physics
a SpringerOpen Journal

REVIEW Open Access

Application of texture analysis to muscle MRI: 2 – technical recommendations

Richard A Lerski[1*], Jacques D de Certaines[2], Dorota Duda[3], Wlodzimierz Klonowski[4], Guanyu Yang[5,6], Jean Louis Coatrieux[7,8,9], Noura Azzabou[2] and Pierre-Antoine Eliat[10]

* Correspondence:
r.a.lerski@dundee.ac.uk
[1]Medical Research Institute, Ninewells Hospital, Dundee, Scotland, UK
Full list of author information is available at the end of the article

Abstract

A goal of the multicenter European Cooperation in Science and Technology (COST) action MYO-MRI is to optimize Magnetic Resonance Imaging Texture Analysis (MRI-TA) methods for application in the study of muscle disease. This paper deals with recommendations on the optimal methodology to collect the MRI data, to analyse it via texture analysis and to make conclusions from the resultant texture parameter data. A full and detailed description is provided with respect to MR image quality control, sequence choice, image pre-processing, region of interest selection, texture analysis methods and data analysis. A series of conclusions are presented.

Keywords: Skeletal muscle; MRI; Texture analysis; Muscle dystrophy; GRMD

Review

Texture of an image region can be defined as describing the spatial relationship of pixel (or voxel) grey shades within that region. It was established in the 1970s [1] that textures could discriminate image regions and that high order properties not accessible to visual appreciation could be detected via computer analysis. Originally, the application was in aerial and geological image interpretation but, since then, there has been an expansion of application into many diverse fields.

Texture analysis (TA) of MR images has been demonstrated to be of clinical value in a wide range of situations [2]. This includes the brain, the liver, the kidney, the breast, the prostate, bone but also muscle [3-6]. There are also some other pre-clinical results in muscle MRI-TA [7-10]. All these results are presented in the First of these joint papers.

This article presents a series of recommendations for performing such MRI TA measurements in vivo for muscle and for analyzing and interpreting the results.

Fundamentally, texture analysis deals with regions of an image and often these are user defined as *regions of interest* (ROIs) for 2D TA, and *volumes of interest* (VOIs) for 3D TA; example applications and results from initial 3D MRI-TA have already been published [5]. The ROIs may be drawn to encompass single tissue types or placed on the image as simple squares/cubes or circles/spheres. Studies that use texture properties can distinguish changes as a disease, for example, progresses but must be trained to know what the significance of the change is against a gold standard eg. Pathology. A

very wide range of TA procedures have been developed, providing many possibilities for investigation in different studies.

Preliminary MRI quality assessment

Quality assessment of MR imaging equipment has been widely developed over the last twenty years [11-15]. Techniques exist based on the use of test objects, which allow the measurement of the parameters of importance in ensuring a constant quality of imaging performance. Without a systematic programme of quality assessment it is impossible to ensure that diagnostic usefulness will be maintained. This is particularly the case when quantitative measurements (such as texture analysis) are attempted on a repeated basis over a period of time.

For the purposes of texture analysis the following quantities are the most important to assess: Firstly signal-to-noise, secondly spatial resolution, and thirdly image uniformity. Additionally it is useful to assess image contrast (dependence on relaxation time variation) and it is also possible to construct texture test objects. There are well established test object methods for investigating these parameters. Before commencement of a TA study a baseline of such measurements should be established. During the study regular checks of these parameters should be made and significant changes addressed.

The signal-to-noise (SNR) of an MR system is most easily assessed through the use of a flat field test object. The simplest technique is to place a square or circular ROI within the image of the test object (see Figure 1) and calculate the mean and standard deviation of the pixel values within it. The Ratio of Mean to Standard Deviation gives a measure of SNR.

However, it is common practice now that it is better to acquire two images under identical conditions (Figure 2) and subtract the two to determine the noise within the same ROI. This procedure removes the influence of image uniformity on the result.

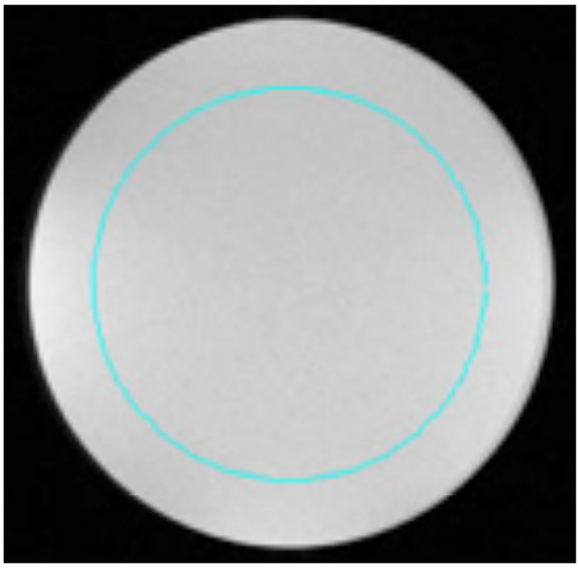

Figure 1 An MR image of a flat field test object (Eurospin TO1) showing a possible choice of circular ROI to calculate a signal-to-noise measure.

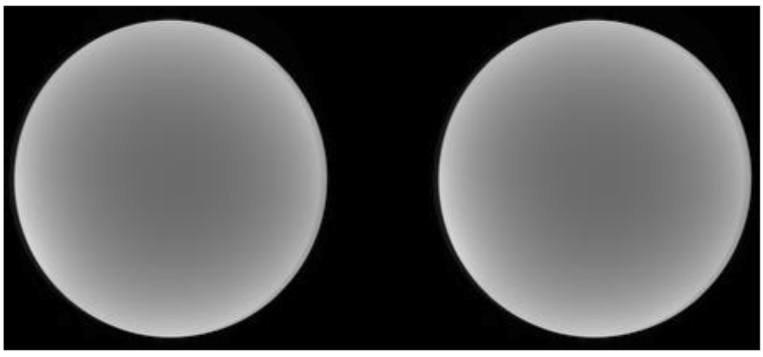

Figure 2 Two MR images of a flat field test object (Eurospin TO1) which may be subtracted to calculate a signal-to-noise measure.

The SNR is then calculated as $\sqrt{2}$ times the ratio of the Mean in the signal image divided by the standard deviation in the subtracted image. The problem with this can be the ability to calculate subtracted images or the standard deviation on the MRI scanner console.

The image uniformity (or homogeneity) can be assessed through use of the same flat field test object. Homogeneity may vary dependent on the precise MR imaging strategy used and this may affect texture results dependent on the normalisation strategy implemented.

It is common in modern scanners for image processing filters to be applied to improve the image uniformity so it is important to be consistent in the application of such filters during any study. Users may need assistance from equipment manufacturers to determine (or alter) the filters in use. Further, it is important to be sure that scanner software upgrades do not alter these filters and again the assistance of manufacturers is required. Quantitation of the uniformity may be done through the use of profiles drawn across these images. It is necessary to use horizontal and vertical profiles since there may be variation between the frequency encoding and phase encoding directions.

The spatial resolution can be investigated through the use of a test object that includes bar patterns (see Figure 3) with appropriate spacings. The Eurospin TO4 [12] is illustrated in Figure 3.

The resolution of the MR system should be determined by the field of view divided by number of pixels in the image matrix. For example a 250 mm field of view and pixel matrix of 256 x 256 should produce a resolution of just less than 1 mm.

The contrast of MR imaging systems can be investigated through the use of a test object such as the Eurospin TO5. This allows the use of 12 glass tubes with varied (but known) T1 and T2 relaxation times. The tubes contain agarose gels of varying 'thickness' (which alters T2) and varying paramagnetic doping (which changes T1). A typical image is shown in Figure 4. Dependent on the sequence used the contrast obtained will vary and can be measured and compared with expected values.

It is possible to construct texture test objects using foam materials with agarose gel filling material. Such a phantom does not completely mimic the structure of muscle (lack of directional properties) but is useful in testing MRI-TA methods.

In the examples shown in Figure 5, foam with specific porosities of 30, 45, 75 and 90 pores per inch (ppi) was sourced to use in a test phantom (Foam Engineers Ltd.;

Figure 3 An MR image of the Eurospin TO4 test object which allows the assessment of image spatial resolution.

Buckinghamshire, UK). The foam samples were submerged in tubes filled with a 2% agarose solution (Sigma Aldrich; St. Louis, MO) held at 70°C. The agarose was doped with 0.2% Magnevist (Bayer Healthcare; Germany) to shorten T1 relaxation times to values comparable with those measured in vivo.

It can be seen that there is no visual difference between the four foams in the MRI image given in Figure 6. Texture analysis could, however, discriminate perfectly between these foams. That is, a classifier using texture results could discriminate between the foams with no errors.

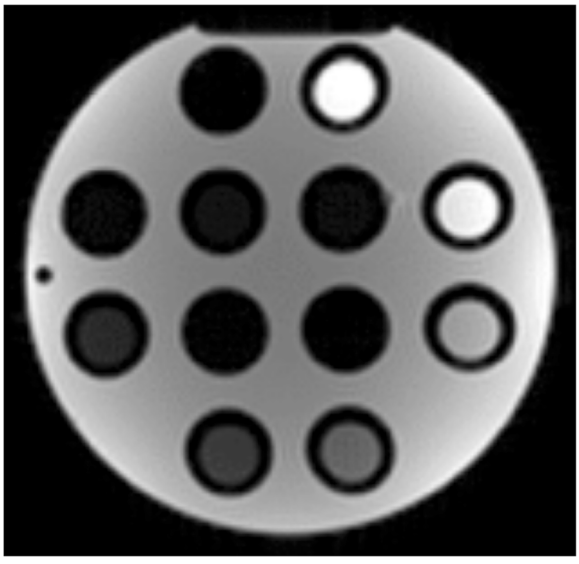

Figure 4 An MR image of the Eurospin TO5 test object which allows the assessment of image relaxation time contrast.

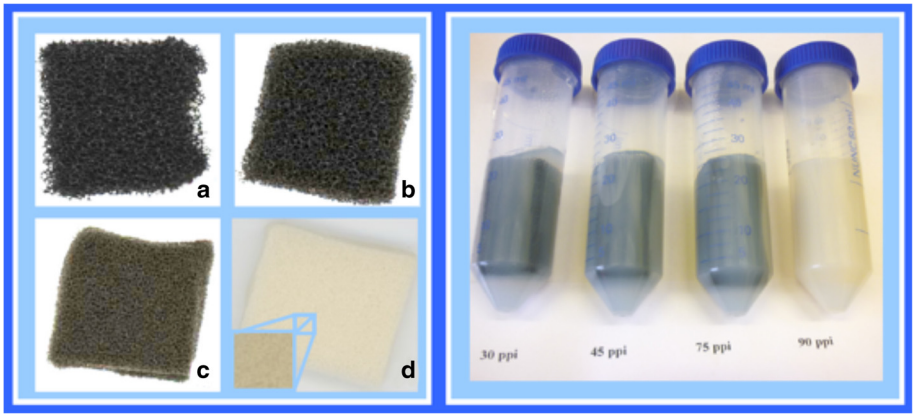

Figure 5 The use of reticulated foam samples to provide image texture variations in MR imaging. The differing foam samples are inserted in plastic tubes and filled with doped agarose gels. Panels on the left show close-ups of the actual foam samples and panels on the right show the foams inserted in the tubes.

Coils and reconstruction

Since the Signal to Noise Ratio (SNR) is a key feature when designing an MRI protocol, the choice of the most suited coils is really crucial. Depending on the body part that is explored several coils configurations can be used, including transmit/receive coils or separate coils for transmission and reception. This latter configuration is often used with surface coil to explore muscles around articulations (knee, elbow, wrist, etc.). These surface coils are an efficient solution to optimize SNR in a small region. Away from this specific area, the sensitivity of the coil decreases very fast. From the Biot-Savart law one can consider that the decrease for simple loop coil can be roughly approximated as $1/z^3$, z being the distance from the centre of the coil, which may influence the texture features in the direction of the gradient (Figure 7)

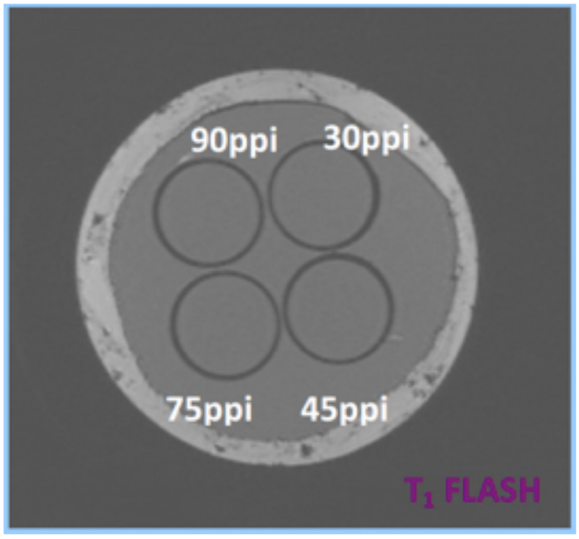

Figure 6 An MR image of the 4 tube texture test object. There is no visual difference between the tube images but image texture analysis can discriminate between them perfectly. This object is extremely useful for studies of how texture results vary with image acquisition changes.

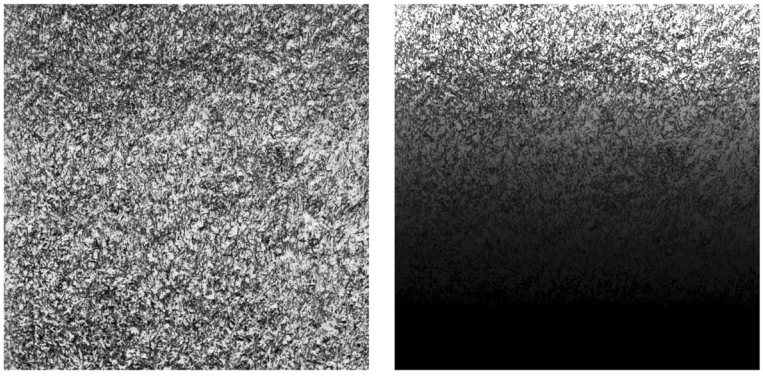

Figure 7 Illustration based on a Brodatz texture (P. Brodatz, "Textures: A Photographic Album for Artists and Designers", Dover Publications, New York, 1966) of the sensitivity coil profile. On the left, the original Brodatz texture. On the right the same texture modified by applying a typical surface coil gradient. Near the coil, the sensitivity is optimal and consequently SNR is increased, while away from the coil centre, the signal decreases.

The extension of this approach is a phased-array coil, which is a combination of multiple coil elements. These coils provide a better sensitivity than a classical RF coil by exploiting the individual high sensitivity of each coil element, but the associated sensitivity map is much more complex and involves many image corrections. These more complex and efficient coils are widely available on clinical systems and are now associated with parallel imaging acquisition strategies that allows shorter acquisition time for a given SNR. Once again, image reconstruction is then much more complex and associated with many (not always editable) options and filters when designing the acquisition protocol on the MRI console. The knowledge and control of all these parameters is not straightforward and can induce bias in the context of quantification and biomarker identification, including texture features.

MRI pulse sequences

The selection of the pulse sequence for MRI acquisition is a key point in the strategy for MRI-TA. Several tissue MR parameters determine the grey level in each voxel: the spin–lattice relaxation time T1, the spin-spin relaxation time T2, the spin density N(H) and the spin displacements (flow and diffusion). Generally for TA the spin echo pulse sequence has been used but fat suppression may also be used (see below). However, the interpretation of voxel grey level is highly complex and must be prudently related to histological changes.

Then the challenge is to develop a pulse sequence potentially able to differentiate histological changes. For instance, to discriminate other modifications from fat infiltration, several fat suppression pulse sequence can be used: short-tau inversion recovery (STIR) [16] has been used to detect muscle edema in DMD though STIR suppresses the signal of all tissues with a short T1 and not selectively the fat. Another pulse sequence, chemical shift selected imaging (CHESS) [17] can provide a selective suppression of fat signal and can be combined with a T2 weighted (T2w) imaging [18]. Chemical shift water–fat separation methods such as multipoint Dixon [19] and iterative decomposition of water and fat with echo asymmetry and least-squares estimation

(IDEAL) [20] separate the water signal from the fat signal using the known phase shift that occurs due to the different precessional frequencies of fat and water. The IDEAL method has also been combined with a Carr–Purcell–Meiboom–Gill (CPMG) imaging sequence to create the IDEAL-CPMG method providing a pair of fat and water decomposed images at each echo time; the water-isolated and fat-isolated signals can then be fitted directly with monoexponential decay curves to measure the T2 of water and the T2 of fat [21]. If fat is totally suppressed, T2 is then a strict water T2; however, fat is not often correctly suppressed minimizing the expected difference between T2 (fat + water) and theoretical water T2. As well, the difference between calculated T2 (the true T2) image, more difficult to obtain and often more noisy, and a T2 weighted (T2w) image must not be underestimated [22].

Different pulse sequences, T1w, T2w, fat-suppressed T1w pre and post contrast agent injection have demonstrated T2w/T1w, T2w and maximal signal enhancement post contrast agent as the more discriminating parameters in dystrophic dog muscle [23]. The images below (Figures 8, 9, 10, 11, 12) illustrate the results obtained with differing pulse sequences in the case of axial slices of the thighs of patients with Pompe disease. Pompe disease is an metabolic disorder which damages muscle and nerve cells throughout the body. It is caused by an accumulation of glycogen in the lysosome and manifests itself through muscle weakness. Muscle texture is affected by this change to tissue structure.

As muscle stiffness is modified in dystrophy, its in-vivo measurement could be relevant. An MR in-vivo method initially proposed in a paper submitted in 1994 and published in 1995 [24], later called Magnetic Resonance Elastography (MRE) [25], has been tested [26]. However, the low resolution which is obtained in MRE make the images without great interest for MRI-TA.

Another MRI method, diffusion tensor imaging (DTI), can provide some geometrical information on fiber size and orientation in muscle dystrophy, as also can MRI-TA [27]. However, DTI in muscle dystrophy is not relevant if the modification caused by the disease is a larger distribution of fibre sizes but with approximately the same mean value, and furthermore the images can be artefacted by fat infiltration.

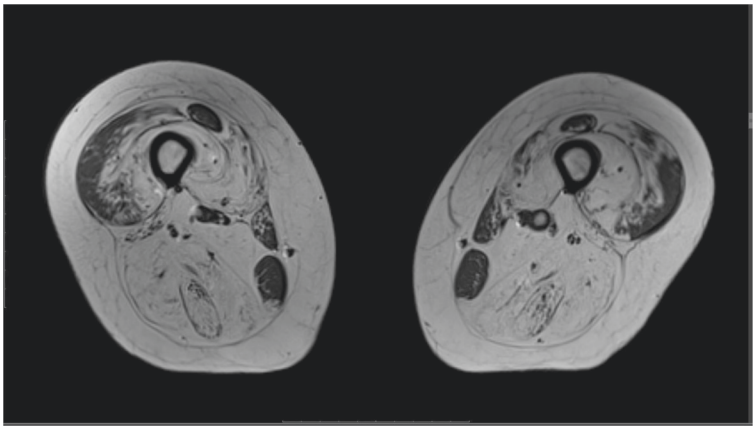

Figure 8 MR image of the thighs of a patient with Pompe disease – T1 weighted.

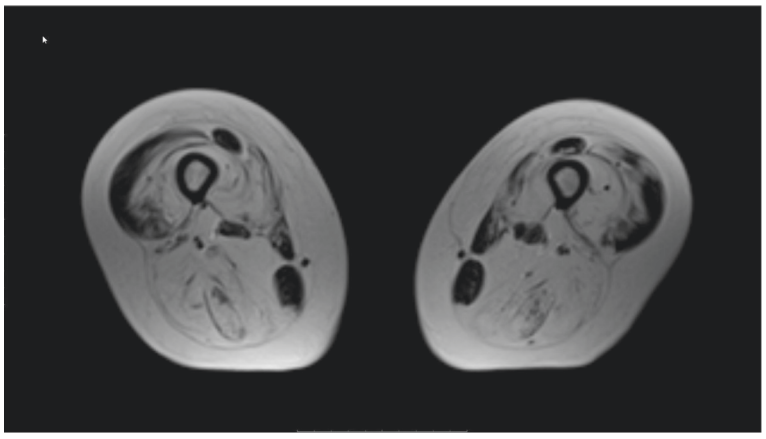

Figure 9 MR image of the thighs of a patient with Pompe disease – T2 weighted.

In summary, the MR pulse sequence selection for MRI-TA has first to take into account the relevance to histological variations, which are not the same during a disease evolution. The total acquisition time is also important, especially with human patients without anesthesia, but is determining for signal-to-noise ratio (SNR) and consequently to spatial resolution: the voxel size (pixel surface x slice thickness) is important; it must be increased to have a better SNR and decreased to have more texture information. Fortunately, as muscle fibers are oriented in a same direction, the slice thickness can be increased if the slice selection is transverse in reference to the main fibers orientation.

Preprocessing (normalization, dynamic range)

In order that TA measurements may be comparable between MR systems (or between different systems) it is necessary to consider whether the image data should be normalised in some manner. Raw image data coming from the scanner will be subject to variations in the electronic gain of the receiver and so the first order amplitude of the image

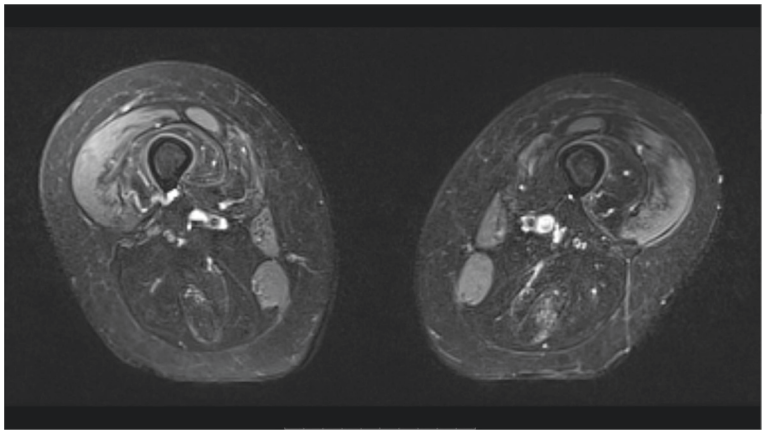

Figure 10 MR image of the thighs of a patient with Pompe disease – T2 weighted with fat saturation used.

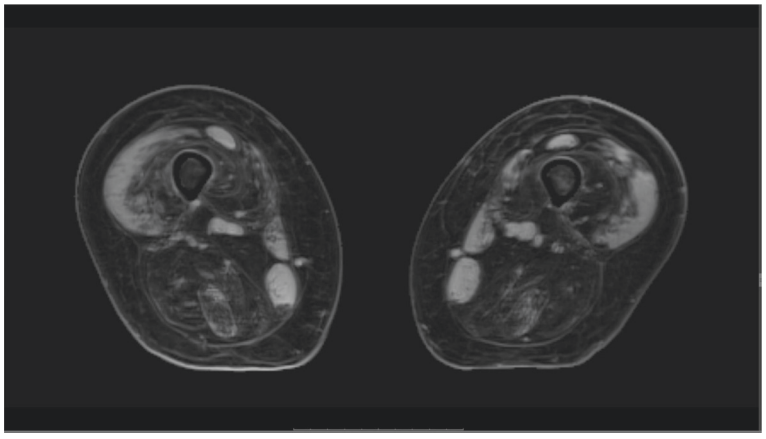

Figure 11 MR image of the thighs of a patient with Pompe disease – water map via 3 point Dixon technique.

(*brightness*) may vary. Further the range of grey shade values (*contrast*) may also vary. Usually the user has no control over the receiver gain, as this setting is automatically set by the scanner software, during set up.

There are many possible approaches to such a normalisation procedure [28]. One common option is to constrain the histogram of the ROI under consideration to a constant image mean and maximum variation of plus and minus 3 times the standard deviation of the pixel values. This is done by adjustment of the software gain and baseline value.

Another matter of great importance in setting up the TA procedure is the number of bits within the image data (dynamic range). It is common in modern MR equipment for the signal data to be digitized to at least 16 if not 24 bits. For several of the common TA procedures eg calculation of the co-occurrence matrix it is undesirable to proceed with this number of bits in the image matrix. This is for two reasons viz. firstly computational complexity is somewhat increased and secondly a resultant sparseness

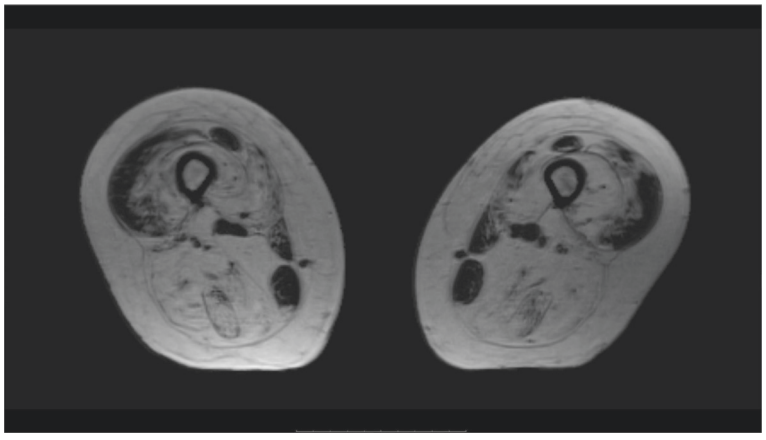

Figure 12 MR image of the thighs of a patient with Pompe disease – fat map via 3 point Dixon technique.

of the resultant co-occurrence matrix, which leads to a sensitivity to noise. A common choice is a reduction of the number of bits in the image to 6 or 8 bits simply by rescaling [29].

Signal-to-noise variations between scanners (different field strengths or receiver characteristics) will also potentially alter texture results. In order to equalize results it may be necessary to consider variation of the NEX (averaging) during acquisition. Increasing NEX obviously increases acquisition time, which in clinical situations, is undesirable.

Window sizing and shaping issues

In the case of TA studies of muscles a choice has to be made between utilising automatic segmentation methods [30] or manual segmentation. As suggested by several authors, the MRI-TA results are often hampered by lack of robust automated muscle segmentation methods [31]. Manual segmentation by the same 'expert' allows better comparisons between texture methods but automated methods are more desirable for clinical use. This issue is still unresolved and requires further work.

There are a number of considerations that determine the choice of Region-of-Interest (ROI) windows for estimating texture features such as the objectives pursued, the nature of the texture and the methods applied for their characterization. The options we have are either geometrical shapes (square or circle windows in 2D, cube or sphere in 3D) or free-form 2D/ 3D shapes (obtained by means of a prior segmentation). These questions are briefly surveyed in this section.

Texture features may be used as a component contributing to automatic object segmentation. In such case, they are combined with edge information in order to improve the extraction results. They are aimed at differentiating the inside from the outside properties of the regions/volumes of interest. Rough estimations of simple features (e.g. first order statistics of image intensities) over geometric windows with small preset sizes are often used. A similar situation is encountered when tracking objects or regions over time like in image sequences. However, if the motion involves also object/region deformations (affine transformation, for instance), invariance of texture features to these deformations should be considered.

Although segmentation, tracking and deformation are of relevance in medical imaging, the main goal remains to precisely characterize the underlying tissue organization and its functional behavior. Such characterization is supposed to be effective in discriminating normal and diseased tissues and needs a large enough number of pixels. Unfortunately, the anatomical structures of interest correspond in general to small-sized objects and have complicated shapes. Geometric windows (as mentioned above) can be interactively placed by the expert. They can also be automatically defined if a prior segmentation has been performed, the size and place of the window being determined by avoiding contour/boundary pixels. However, a manual delineation is often required to extract the target tissue structures in the images. This delineation is not error-free and may involve several experts for cross-validation. This manual interaction becomes highly time-consuming when performed on all the slices of concern. Despite the fact that we have access to the 3D information, e.g. the right dimensional space to work into for tissue texture, in most cases only 2D processing is carried out due to the poor resolution in thickness and between slices. It is also the case that true 3D image

acquisitions are extremely time consuming and are unlikely to be practical in a clinical setting. Parallel encoding techniques with gradient echoes do allow 3D acquisitions but this has not, so far, been tested in conjunction with MRI-TA.

In addition, the classical views applied to the nature of textures (structured versus random) may fail to capture the complexity of tissue textures. To get reliable descriptive parameters in the case of structured texture, the window size must be set according to the periodicity of the pattern. Such pattern is not frequently observed in medical imaging. High order statistical parameters computed in the case of random texture require enough pixels to reduce the potential biases. Texture mixtures may also complicate the feature estimations and increase the number of pixels needed. The inherent presence of noise is another critical issue. Noise refers to the intrinsic property of the imaging device and to the interaction between physical waves and tissues. Here too, Gaussian and Laplacian distributions of noise are widely assumed for the definition of samples (e.g. pixels) but are far from being verified in practice.

Summarizing, window sizing and shaping are driven by the data acquired, the nature of the texture, the noise level and type, the texture methods applied and the target we have. Compromises must be carefully examined. Local windows with predefined sizes and shapes, either sliding or not according to the extent of the regions of interest, are most often used. They must have enough pixels in order to get accurate texture feature estimates. 3D TA requires a greater number of voxels not always compatible with the size of the clinical area under examination. For instance, there are nearly 30000 voxel of 1 mm3 in a VOI of 31×31×31 mm. High-order statistics are more sensitive to noise and must be carefully handled. Global windows or bounding boxes of the regions of interest represent another solution but require consideration of proper methods to separate texture from shape.

Overview of the different TA methods

The following describes the various options for methods to investigate the texture properties of digital images. The general categories of the methods are statistical, filter based and model based. Many of the methods can be implemented both in 2D and 3D.

Statistical methods

Grey-level histogram (GLH) - based method

This method allows the calculation of first-order features, based only on the distribution of grey levels (or intensities) of pixels within an analyzed ROI. Such features provide knowledge on the most and the least occurring grey levels, on the concentration of the grey levels around their average, or on the degree of asymmetry in their distribution. Contrariwise, they contain no information on the relationship between neighboring pixels, on the possible direction of the texture, its structure, and other properties resulting from these relationships.

Features

Four features are the most frequently obtained from a grey-level histogram:

- *Average grey level*, *mean of grey levels*: measure of darkness (or brightness) of the image. It represents the location of the histogram on the grey-level scale.

- *Variance of grey levels*: characterizes the distribution of grey levels around the mean.
- *Skewness*: measures of the asymmetry of the grey-level histogram. It expresses a deviation of the grey-level distribution, compared to a symmetric one. It is equal to zero for the symmetric histograms, negative for right oriented ones (high grey levels are more frequent) and positive for a left oriented histograms (more frequent low grey levels).
- *Kurtosis*: indicates the relative flattening of the grey-level distribution. It is equal to zero for a normal distribution. It takes a negative or a positive value for a distribution whose graph is relatively flat or relatively sharp, respectively.

Autocorrelation (AC) - based method

The correlation between the grey levels of neighboring pixels can be expressed by the normalized autocorrelation coefficients [32]. It is the function of the vertical (Δx) and the horizontal (Δy) distance between the considered pixels in pairs, and can be defined as follows: $\gamma(\Delta x,\Delta y) = A(\Delta x,\Delta y)/A(0,0)$. $A(\Delta x,\Delta y)$ is the average product of pairs of grey levels corresponding to all the pairs of pixels belonging to a ROI, and spaced from one another by a distance $(\Delta x,\Delta y)$. To make the autocorrelation coefficient independent of the image brightness, the grey level mean can be extracted from each grey level before calculating the above formula.

Features

The normalized autocorrelation coefficients can be regarded as textural features. They provide information about the spatial relationship between the texture patterns. For small primitives (texture elements), autocorrelation changes rapidly with change in the distance between the pixels. For the large primitives, it changes slowly. The presence of regular patterns makes regular periodic changes in the autocorrelation.

Gradient (G) - based method

The grey-level gradient at a particular image point depends on the differences between the grey levels of its neighboring pixels, arranged on vertical and horizontal lines intersecting at this point. In most cases, a neighborhood of 3×3 pixels or 5×5 pixels is considered. The gradient matrix contains the values of the absolute gradient at each point of the ROI, except for its boundaries.

Features

On the basis of the gradient matrix, the following features can be calculated [33]: *mean*, *variance*, *skewness*, and *kurtosis*. Such features allow us to draw conclusions about the uniformity (homogeneity) or the roughness of the texture. They may also indicate the presence or absence of edges within the ROI.

Grey-level difference matrix (GLDM) - based method

The method consists in studying the absolute values of differences between the grey levels of pixels in pairs belonging to a ROI [34]. Four pixel alignment directions, θ (0°, 45°, 90°, and 135°), and different distances, d, between the pixels in pairs can be considered. The most often, d takes small values. A combination (d,θ) determines the relative position of pixels composing the pairs to analyze. For a specified combination (d,θ), all possible absolute differences in grey levels that can be encoded in the image are taken into account. For each absolute difference, the probability of occurrence of a pair of pixels with just such a difference in the grey levels is calculated. The probabilities

sorted in increasing order of corresponding absolute grey level differences form a vector $\mathbf{l}(d,\theta) = [l_0, l_1,\ldots,l_{G-1}]^T$, where G is the number of grey levels possible to occur in the image.

If the distances, d, between pixels in the considered pairs are small, compared to the texture primitives, the grey levels in pairs are quite similar. In this case, the initial components of $\mathbf{l}(d,\theta)$ vector have high values, while the last ones are close to zero. Conversely, if d approaches the texture primitives size, the probabilities of small differences in pixel grey levels are much smaller, and the components of $\mathbf{l}(d,\theta)$ are more spread out. Further, if a texture is directional, the distribution of probabilities in $\mathbf{l}(d,\theta)$ will be different for different θ values. Conversely, if the texture does not seem to have any particular directional elements, the distribution of probabilities in $\mathbf{l}(d,\theta)$ is not significantly affected by the θ.

Features

Five textural features can be derived from the $\mathbf{l}(d,\theta)$ vector. Comparing their values obtained for different pixel distances and/or pixel alignment directions one can draw conclusions about the size, the quantity, and the orientation of texture primitives.

- *Mean* is small for fine textures, when the probabilities of small grey level differences are high, and it is large for diversified textures giving high probabilities of big differences.
- *Energy* or *angular second moment* is small when all the probabilities in the $\mathrm{l}(d,\theta)$ vector are similar (fine textures), and large when some vector components are high, and others low.
- *Contrast* or *inertia* is a measure of intensity contrast between a pixel and its neighbors. It is equal to zero for a constant image, and reaches high values for images with extremely differing grey levels.
- *Inverse difference moment* is the measure of the *local homogeneity*.
- *Entropy* is large for the images that are texturally not uniform, when all the probabilities in the $\mathrm{l}(d,\theta)$ vector are close to each other. The more the probabilities in vector are diversified, the smaller is the entropy.

For non-directed textures, features obtained with the same formula, for the same d, but corresponding to different alignment directions of pixel pairs, θ, can be averaged. Alike, it is possible to average features calculated for different distances.

Co-occurrence matrix (COM) - based method

A co-occurrence matrix $\mathrm{C}(d,\theta)$ is also constructed for a given distance, d, between pixels, still considered in pairs, and a given pixel alignment direction, θ. Each element, c_{ij} $(i,j = 0,\ldots,G\text{-}1)$ represents a probability of occurrence in a ROI of a pair of pixels in which: the first pixel has a grey level i, and the second one – a grey level j [35]. G is the number of grey levels that can be encoded in an image. A matrix dimension is therefore $G \times G$. Like in the GLDM-based method, four pixel alignment directions and several distances between pixels could be considered. In contrast to the previous method, a COM-based one focuses on all the possible combinations of grey levels in pairs.

Features

Several parameters were initially proposed in [35]:

- *Energy* or *angular second moment* is a measure of homogeneity of grey levels characterizing the pixels of a ROI. For relatively homogeneous textures, the grey levels of adjacent pixels are similar. In this case, larger probabilities are associated with elements located on the diagonal (or very close to the diagonal) of the co-occurrence matrix, the other matrix elements are close to zero. The energy for homogeneous textures is greater than for the heterogeneous textures. For the latter ones – c_{ij} probabilities are more uniformly distributed throughout the matrix, and their values are quite small.
- *Contrast* or i*nertia*, with a quite large value for heterogeneous regions, characterized by a strong contrast, and quite small value for homogeneous regions.
- *Inverse difference moment* or *local homogeneity*.
- *Entropy*, that quantifies the degree of randomness of the grey levels in a ROI. Its value is the highest when all elements of $C(d,\theta)$ matrix are equal.

Another parameter, *correlation*, can be obtained with the mean and standard deviation of the row and column sums of the $C(d,\theta)$ matrix.

Some other features can be derived from a vector whose components are the co-occurrence probabilities for pixels with a determined sum of the grey levels. All possible sum values are taken into account. The probabilities forming a vector are sorted in increasing order of corresponding sum values. These features are: *sum average*, *sum variance*, and *sum entropy* [36]. Taking the absolute differences of grey levels, instead of their sums, leads to the features already known from GLDM - based method.

Features calculated for different angles, θ, and/or for different distances, d, can be averaged.

Run-length matrix (RLM) - based method

This method involves counting the number of pixel runs of each grey level, having a given length [37]. All the lengths that can be encountered in the ROI are considered. As in the two preceding methods, four pixels alignment directions, (θ), can be taken into account. The run-length matrix, $R(\theta)$, built for a given θ, has G columns. Each column corresponds to a grey level. In turn, rows of this matrix correspond to all the consecutive run lengths. The number of rows, M, is thus determined by the size of the ROI, and is equal to the maximum length of the pixel run which can exist in a ROI. The element r_{mg} ($r = 1,\ldots,M$, and $g = 0,\ldots,G$) of the matrix $R(\theta)$ is the number of pixel runs of the level g, with the length of m, and oriented in the direction θ.

Homogeneous textures have fairly long pixel runs, while for rough textures, short runs are the most numerous. The features obtained from the RLM method can give the information on the orientation of some texture elements, for example – on the presence of stripes.

Features

The most known features, proposed in the above paper, are: *the short run emphasis*, the *long run emphasis*, the *grey level non-uniformity* (*distribution*), *the run length non-uniformity* (*distribution*), and the *fraction of image in runs*. Two additional parameters were proposed in [38]: *low grey level runs emphasis*, and *high grey level runs emphasis*. Finally, in [39], a *run length entropy was* used as a texture feature.

Filter methods

Laws' texture energy measures

Laws proposed to transform the images using linear filters [40]. An image filtering consists in assigning a new value (grey level) to each pixel of an original ROI, excluding the pixels on its borders. For linear filters such a value depends on a linear combination of the grey levels of the pixels in some neighbourhood of the transformed pixel. The most often two types of neighbourhood are taken into account: 3×3 pixels and 5×5 pixels. The importance of each neighbours contribution to the output pixel value is defined by a mask, called also a convolution matrix. The masks were designed in order to detect different texture elements: ripples, edges, spots.

On the basis of a transformed image, the entropy and several image energy measures can be calculated.

Model-based methods

Fractal model

Several definitions of a fractal object, as well as several methods of calculating a fractal dimension were proposed [41-43]. Benoit Mandelbrot, the creator of fractal geometry, characterized fractals as self-similar objects, whose parts are similar to the whole, and whose topological dimension is not an integer [44]. The fractal dimension of an object reflects the extent to which this object fills the space or the rate of its diversity, the degree of irregularity of the object.

A grey-level image can be considered as a surface in three-dimensional space, where two dimensions are those of the image plane and the third one is the grey level (intensity) of pixels. In this case, we can use the fractal dimension of image surface as a texture descriptor. This feature gives a measure of the irregularity, and of the roughness of the texture. The more a surface is rough, the higher is its fractal dimension.

The fractal dimension of an image (a texture) can be calculated by representing the intensity surface of an image by a fractional Brownian motion model (see also [36]). One of its applications for texture feature extraction can be found in [45].

Image landscapes' fractal dimension (ILF) method

The **ILF** method is based on constructing from the analyzed 2-D grey level images two 1-D sequences that are called *landscapes.*

Stepping through a grey value image length of N pixels and height of M pixels row by row one can calculate the sum of the grey values in each row, G_m $(m = 1, \ldots, M)$, and dividing these numbers by the largest of them, G_R, we obtain the *horizontal landscape, hgs,*

$$NGS_m = G_m/G_R \in [0,\ 1] \qquad m = 1, \ldots, M \tag{1}$$

where $G_m = \sum_{n=1}^{N} g_{mn}$ $G_R = \max(G_m)$ $\qquad m = 1, \ldots, M$

Similarly, stepping through the same image column by column one can calculate the sum of the grey values in each column, G_n $(n = 1, \ldots, N)$, and dividing these numbers by the largest of them, G_C, we obtain the *vertical landscape, vgs*

$$NGS_n = G_n/G_C \in[0,\ 1] \qquad n = 1, ..., N \tag{2}$$

where $G_n = \sum_{m=1}^{M} g_{mn}$; $G_C = \max(G_n)$ $\qquad n = 1, ..., N$

The landscapes obtained in such a way are then analyzed using Higuchi fractal dimension in a sliding window of the length L moved in each step l points (pixels) to the right. Normalization in (1) and (2) is convenient but not really necessary since Higuchi fractal dimension is invariant with respect to scaling of the data.

Features

Using ILF method [46] one can obtain the following characteristics of the analyzed image:

- *Two (or four) graphs of fractal dimension* of the image, along horizontal and vertical axes; if fractal dimension smoothly fluctuates it means that there are non-stationarities/discontinuities in the image; in such a case mean fractal dimensions D_h and D_v are enough to characterize the image.
- *Two (or four) mean fractal dimension values* – if their values are nearly identical then it is enough to characterize the surface (its image) using one number, D_f – the average of D_h and D_v; if D_h and D_v differ considerably it means that the surface (and so its image) shows texture, i.e. has different properties in different directions.

Moment-based methods

These methods belong to the so-called transform methods. They include several families among which complex moments, rotational moments, geometric moments and orthogonal moments are the quantities studied [47-49]. Orthogonal moments, such as Legendre and Zernike moments, present the advantage of being optimal with regard to information redundancy. To provide some cues on these moments, let us take the example of Legendre moments. The two-dimensional (2D) $(n + m)$th order of Legendre moment of an image intensity function $f(x, y)$, L_{nm}, is defined as

$$L_{nm} = \frac{(2n+1)(2m+1)}{4}\int_{-1}^{1}\int_{-1}^{1} P_n(x)P_m(y)f(x,y)dxdy \tag{3}$$

where $P_n(x)$ is the nth order of Legendre polynomial given by

$$P_n(x) = \frac{1}{2^n}\sum_{k=0}^{n/2}(-1)^k \frac{(2n-2k)!}{k!(n-k)!(n-2k)!}x^{n-2k} \tag{4}$$

Since the Legendre polynomials are orthogonal over the interval [−1, 1], the image $f(x, y)$ (the ROI in most cases) can be reconstructed from its moments. When an analog original image is digitized to its discrete form, the 2D Legendre moments L_{nm} defined by Eq. (3) is usually approximated by

$$L_{nm} = \frac{(2n+1)(2m+1)}{(N-1)(M-1)}\sum\nolimits_{i=1}^{N}\sum\nolimits_{j=1}^{M} P_n(x_i)P_m\left(y_j\right)f(i,j) \tag{5}$$

with $x_i = \frac{2i-N-1}{N-1}$, $y_i = \frac{2j-M-1}{M-1}$.

Features

The texture features are in such case the estimated coefficients $L_{nm.}$ The number of features depends on the order selected. The low order coefficients capture the low

frequency components while the high order ones (more sensitive to noise) will provide details of the image or the ROI under consideration.

Data analysis

Once a series of texture features are extracted it is necessary to determine the usefulness of each or combinations of several for a particular classification task. This is often called *pattern recognition* or *data mining* and consists of applying well-developed methods to determine how the features can be used to classify the data. The overall objective of the data mining process is to extract information from a data set and transform it into an understandable structure for subsequent use.

There are a large number of methods which can be applied to these problems eg discriminant analysis, principal component analysis, clustering, neural networks etc. etc. It is not the purpose of this paper to review these in any detail. There are also a significant number of commercial (or freeware) software packages that are available to help with these tasks. Examples of these are Weka, SPSS, The Unscrambler, SAS and STATISTICA.

As an example, Weka is a collection of machine learning algorithms for data mining tasks. The algorithms can either be applied directly to a dataset or called from a users own Java code. Weka contains tools for data pre-processing, classification, regression, clustering, association rules, and visualization. It is also well-suited for developing new machine learning schemes.

Using computers for texture segmentation and analysis, both supervised and unsupervised, is obvious but it raises some questions. The most important question that biomedical researchers have been asked since computer introduction to the labs is '**Do you REALLY understand what your computer calculates?**' Unfortunately, the answer to this question is quite often not positive. It concerns in particular commercial software when the source code is not given to the end users and even IT specialists often have problems with understanding the details of source code written by others. In the case of Biologists and Medical Doctors there is a problem with interpretation of texture parameters, which have little intuitive meaning.

The second question concerns **repeatability of results**. One would like that at least classification of the images from a given series would lead to the same result when repeated. But already the problem of choosing the Region(s) of Interest may lead to differences between researchers. It seems that the whole image is as unbiased as one can get, any remaining bias originated in how the images were acquired. It was exactly the case in the application of a fractal method in the analysis of textures of anatomo-pathological slides for staging in cases of Anal Intraepithelial Neoplasia [46] - some original slides showed white irregular 'holes' but any attempts to analyze ROIs without these holes only worsened the final results.

The third question concerns very, very important but not well-known so called '**The Curse of Dimensionality**'. To create a classifier first one needs descriptors for each object class that can be expressed by numbers. It might seem that to obtain a more accurate classification, one could add more features, maybe even a few hundred of these features. But in fact, after a certain point, increasing the dimensionality of the problem by adding new features would actually degrade the performance of the classifier - as the dimensionality increases, the classifier's performance increases until the optimal number of features is reached; further increasing the dimensionality without increasing the number of training samples results in a decrease in classifier performance; this is called **overfitting** (see [50]). So, with only a small number of images in the database, it is just intractable to check

all possible combinations of features in any given method nor to compare different proposed methods of texture analysis to decide which combination or which method is the best one. Even so called feature extraction methods like Principal Component Analysis, that reduce the dimensionality of the classification problem, are not always helpful.

In summary, complicated and very specialized methods are good for research studies (with care over over-interpretation), but if one wants to propose a texture analysis procedure that could become widely applicable in hospitals and clinics, this should be a rather quite simple method, based on only a few texture parameters (preferably just one or two), quick and easily understandable by Medical Doctors. More work is required on this latter point.

Conclusion

The review presented in the sections above leads to the following conclusions. The important points that must be considered when applying texture analysis to in-vivo muscles are the following:

1. Quality assessment of the MR imaging system is essential both at the beginning and throughout any study
2. Careful choice of imaging sequence is required with regard to image resolution, imaging time and signal-to-noise.
3. Many kinds of texture analysis methods exist. To ensure that the best results are obtained, a full range of procedures should be investigated.
4. The Regions of Interest used for the texture analysis should not be too small (>100 pixels in 2D TA)
5. The dynamic range (pixel depth) of the MR images will need to be reduced to allow practical texture analysis to be carried out. Eight or six bits are recommended.
6. Normalisation of the MR images is essential to remove unwanted variations caused by receiver gain changes.
7. Care must be taken to avoid over-interpretation of the texture data due to the large number of texture parameters and the sometimes limited amount of independent image data available.
8. With all these points taken into consideration, texture analysis carried out on MR images is capable of providing useful clinical information. Progression of disease processes can be followed and muscle status assessed.

If attention is paid to all these factors then the published evidence is that texture analysis of MR data may well be useful in a clinical setting. What is required now is an improved understanding of how the texture results relate to the underlying pathological changes in tissue and also a good way of presenting the output of the texture analysis for interpretation by medical specialists.

Abbreviations

2D: Two dimensional imaging; 3D: Three dimensional imaging; B_0: Static magnetic field of the mri device (in Tesla); CFA: Correspondence factorial analysis; DMD: Duchenne muscular dystrophy; GRMD: Golden retriever muscular dystrophy; I Signal: Intensity; MHz: Mega hertz; MRI: Magnetic resonance imaging; NEX: Number of excitations in MRI acquisition; NMR: Nuclear magnetic resonance; N(H): Spin density; PCA: Principal component analysis; ROI: Region of interest; SE: Spin echo pulse sequence; SNR: Signal to noise ratio; TA: Texture analysis; TO: Test object; TR: Repetition time in MRI acquisition; T1: Spin lattice NMR relaxation time; T2: Spin spin NMR relaxation time; VOI: Volume of interest.

Competing interests
The authors declare that they have no competing interests.

Authors' contributions
All authors have contributed to the manuscript, which has been finally edited by RAL. All authors read and approved the final manuscript.

Author details
[1]Medical Research Institute, Ninewells Hospital, Dundee, Scotland, UK. [2]Institute of Myology, University Hospital Pitié-Salpêtrière, Paris, France. [3]Faculty of Computer Science, Bialystok University of Technology, Bialystok, Poland. [4]Nalecz Institute of Biocybernetics and Biomedical Engineering Polish Academy of Sciences, Warsaw, Poland. [5]Laboratory of Image Science and Technology, School of Computer Science and Engineering, Southeast University, Nanjing 210096, China. [6]Centre de Recherche en Information Biomédicale Sino-français (CRIBs), Nanjing, China. [7]INSERM, U1099, Rennes F-35000, France. [8]Université de Rennes 1, LTSI, Rennes F-35042, France. [9]Centre de Recherche en Information Biomédicale Sino-français (CRIBs), Rennes F-35000, France. [10]PRISM-Bio-SCANs, University of Rennes, Rennes, France.

Received: 10 December 2014 Accepted: 26 February 2015
Published online: 19 March 2015

References

1. Haralick R. Statistical and structural approaches to texture. IEEE Proc. 1979;67:786–804.
2. Hajek M, Dezortova M, Materka A, Lerski R. Texture Analysis for Magnetic resonance Imaging. Prague: Med 4 publishing; 2006.
3. Biondetti PR, Ehman RL. Soft-tissue sarcomas: use of textural patterns in skeletal muscle as a diagnostic feature in postoperative MR imaging. Radiology. 1992;183(3):845–8.
4. Skoch A, Jirak D, Vyhnanovska P, Dezortova M, Fendrych P, Rolencova E, et al. Classification of calf muscle MR images by texture analysis. MAGMA. 2004;16:259–67.
5. Wang J, Fan Z, Vandenborne K, Walter G, Shiloh-Malawsky Y,et al. Statistical texture analysis based MRI quantification of Duchenne muscular dystrophy in a canine model. Proc. SPIE 8672, Medical Imaging 2013: Biomedical Applications in Molecular, Structural, and Functional Imaging, 86720 F (March 29, 2013);
6. Nketiah G, Sievanen H, Eskola H. Correlation between hip muscles MRI texture parameters and femoral neck boneareal bone mineral density (aBMD) in different athletes groups. Phys Med. 2014;30(Supplement 1):e38–9.
7. Herlidou S, Rolland Y, Bansard JY, Le Rumeur E, de Certaines JD. Comparison of automated and visual texture analysis in MRI: characterization of normal and diseased skeletal muscle. Magn Reson Imaging. 1999;17(9):1393–7.
8. Mahmoud-Ghoneim D, Cherel Y, Lesoeur J, Lemaire L, Rocher C, de Certaines JD, et al. Texture analysis of magnetic resonance images of rat muscles during atrophy and regeneration. Magn Reson Imaging. 2006;24(2):167–71.
9. Mamhoud-Ghoneim D, Bonny JM, Renou J-P, de Certaines JD. Ex-vivo Magnetic Resonance Imaging Texture Analysis can identify genotypic origin in bovine meat. J Sci Food Agric. 2005;85:629–32.
10. Nguyen F, Eliat PA, Pinot M, Franconi F, Lemaire L, de Certaines JD, et al. Correlations between Magnetic Resonance Imaging histopathology in mdx (X-linked Muscular Dystrophy) murine model of Duchenne Muscular Dystrophy. Edinburgh: 24th congress of the European Society of Veterinary Pathology; 2006.
11. Lerski RA, de Wilde J, Boyce D, Ridgway J. Quality control in magnetic resonance imaging. IPEM Report no 80. 1998. ISBN: 0904181901.
12. European Communities Research Project (COMAC BME II 2.3). Protocols and test objects for the assessment of MRI equipment. Magn Reson Imaging. 1988;6:195–9.
13. Lerski RA, McRobbie DW, Straughan K, Walker PM, de Certaines JD, Bernard AM. Multi-center trial with protocols and prototype test objects for the assessment of MRI equipment. Magn Reson Imaging. 1988;6:201–14.
14. Lerski RA, de Certaines JD. Performance assessment and quality control in MRI by Eurospin test objects and protocols. Magn Reson Imaging. 1993;11:817–33.
15. Jackson EF, Bronskill MJ, Drost DJ, Och J, Pooley RA, Sobel WT, et al. AAPM Report 100: Acceptance Testing and Quality Assurance Procedures for Magnetic Resonance Imaging Facilities. College Park, MD: American Association of Physicists in Medicine; 2010. ISBN 978-1-936366-02-6.
16. Bydder GM, Pennock JM, Steiner RE, Khenia S, Payne JA, Young IR. The short TI inversion recovery sequence—An approach to MR imaging of the abdomen. Magn Reson Med. 1985;3:251–4.
17. Keller PJ, Hunter WW, Schmalbrock P. Multisection fat–water imaging with chemical shift selective presaturation. Radiology. 1987;164:539–41.
18. Kobayashi M, Nakamura A, Hasegawa D, Fujita M, Orima H, Takeda S. Evaluation of dystrophic dog pathology by fat-suppressed T2-weighted imaging. Muscle Nerve. 2009;40:815–26.
19. Glover GH, Schneider E. Three-point Dixon technique for true water/fat decomposition with B0 inhomogeneity correction. Magn Reson Med. 1991;18:371–83.
20. Reeder SB, Pineda AR, Wen Z, Shimakawa A, Yu H, Brittain JH, et al. Iterative decomposition of water and fat with echo asymmetry and least- squares estimation (IDEAL): application with fast spin-echo imaging. Magn Reson Med. 2005;54:636–44.
21. Janiczek RL, Gambarota G, Sinclair CDJ, Yousry TA, Thornton JS, Golay X, et al. Simultaneous T2 and Lipid Quantitation Using IDEAL-CPMG. Magn Reson Med. 2011;66:1293–302.
22. Carlier PG. Global T2 versus water T2 in NMR imaging of fatty infiltrated muscles: different methodology, different information and different implications. Neuromuscul Disord. 2014;24:390–2.
23. Thibaud JL, Monnet A, Bertoldi D, Barthelemy I, Blot S, Carlier PG. Characterization of dystrophic muscle in golden retriever muscular dystrophy dogs by nuclear magnetic resonance imaging. Neuromuscul Disord. 2007;17:575–84.

24. Lewa CJ, de Certaines JD. Viscoelastic property detection by elastic displacement NMR measurements. J Magn Reson Imaging. 1995;5:242–4.
25. Muthupillai R, Lomas DJ, Rossman PJ, Greenleaf JF, Manduca A, Ehman RL. Magnetic resonance elastography by direct visualization of propagating acoustic strain waves. Science. 1995;269(5232):1854.
26. Qin EC, Juge L, Lambert S, Sinkus R, Bilston L. MR-Elastography and diffusion tensor imaging to measure the in-vivo anisotropic elasticity of skeletal muscles of Mdx and healthy mice. Proc Int Soc Mag Reson Med. 2012;20:3269.
27. McMillan A.B., Shi D., Pratt S.J.P., Lovering R.M., Diffusion Tensor MRI to Assess Damage in Healthy and Dystrophic Skeletal Muscle after Lengthening Contractions, Journal of Biomedicine and Biotechnology, vol 2011, Article ID 970726, 10 pages,
28. Collewet G, Strzelecki M, Mariette F. Influence of MRI acquisition protocols and image intensity normalization methods on texture classification. Magn Reson Imaging. 2004;22(1):81–91.
29. Mahmoud-Ghoneim D, Alkaabi MK, de Certaines JD, Goettsche FM. The impact of image dynamic range on texture classification of brain white matter. BMC Med Imaging. 2008;8:18.
30. Wang J, Fan Z, Vandenborne K, Walter G, Shiloh-Malawsky Y, An H, et al. A computerized MRI biomarker quantification scheme for a canine model of Duchenne muscular dystrophy. Int J Comput Assist Radiol Surg. 2013;8(5):763–74.
31. Fan Z, Wang J, Ahn M, Shiloh-Malawsky Y, Chahin N, Elmore S, et al. Characteristics of magnetic resonance imaging biomarkers in a natural history study of golden retriever muscular dystrophy. Neuromuscul Disord. 2014;24(2):178–91.
32. Gonzalez RC, Woods RE. Image Compression. In: Digital Image Processing. 2nd ed. Reading, MA: Addison-Wesley; 2002.
33. Lerski R, Straughan K, Shad L, Boyce D, Bluml S, Zuna I. MR Image Texture Analysis - An Approach to Tissue Characterization. Magn Reson Imaging. 1993;11:873–87.
34. Weszka JS, Dyer CR, Rosenfeld A. A Comparative Study of Texture Measures for Terrain Classification. IEEE Trans Syst Man Cybern. 1976;6:269–85.
35. Haralick RM, Shanmugam K, Dinstein I. Textural features for image classification. IEEE Trans Syst Man Cybern. 1973;3:610–21.
36. Bankman I. N. (Ed.). Handbook of Medical Imaging, Processing and Analysis, Academic Press, 2000.
37. Galloway MM. Texture analysis using grey level run lengths. Comput Graphics Image Process. 1975;4:172–9.
38. Chu A, Sehgal CM, Greenleaf JF. Use of grey value distribution of run lengths for texture analysis. Pattern Recogn Lett. 1990;11:415–20.
39. Albregtsen F, Nielsen B, Danielsen HE. Adaptive grey level run length features from class distance matrices. Proc 15th Int Conf Pattern Recognition. 2000;3:738–41.
40. Laws KI. Textured image segmentation. Los Angeles, California, USA: Unpublished doctoral dissertation. University of Southern California; 1980.
41. Edgar G. A. Measure, Topology and Fractal Geometry, Springer-Verlag, 1990.
42. Falconer K. Fractal Geometry, Mathematical Foundations and Applications, John Wiley & Sons, 1990.
43. Peitgen H. O., Jürgens H., Saupe D. Fractals for the Classroom. Part 1: Introduction to Fractals and Chaos, Springer-Verlag, 1992.
44. Mandelbrot B. The Fractal Geometry of Nature, W. H. Freeman and Co., 1982
45. Chen EL, Chung PC, Chen CL, Tsai HM, Chang CI. An automatic diagnostic system for CT liver image classification. IEEE Trans Biomed Eng. 1998;45(6):783–94.
46. Klonowski W, Pierzchalski M, Stepien P, Stepien R, Sedivy R, Ahammer H. Application of Higuchi's fractal dimension in analysis of images of Anal Intraepithelial Neoplasia. Chaos, Solitons Fractals (Elsevier). 2013;48:54–60.
47. Shu H, Luo L, Coatrieux JL. Moment-Based Approaches in Image, Part 1. Basic Features. IEEE Eng Med Biol Mag. 2007;26(5):70–4.
48. Shu HZ, Luo LM, Coatrieux JL. Moment-based approaches in image, Part2: invariance. IEEE Eng Med Biol Mag. 2008;27(1):81–3.
49. Shu HZ, Luo LM, Coatrieux JL. Moment-based approaches in image, Part 3: computational considerations. IEEE Eng Med Biol Mag. 2008;27(3):89–91.
50. Vincent Spruyt, About the Curse of Dimensionality, June 6, 2014, http://www.datasciencecentral.com/profiles/blogs/about-the-curse-of-dimensionality.